system used for the Fenske-Hall calculations (8 pages). Ordering information is given on any current masthead page.

References and Notes

(1) (a) Texas A&M University. (b) University of Oxford.
(2) (a) Cotton, F. A.; Haas, T. E. *Inorg. Chem.* **1964,** *3,* 10. (b) Cotton, F. A. *Ibid.* **1965,** *4,* 334.
(3) Cowley, A. H. *Prog. Inorg. Chem.* **1979,** *26,* 45.
(4) Cotton, F. A.; Mague, J. T. *Inorg. Chem.* **1964,** *3,* 1402.
(5) Gehrke, H., Jr.; Bue, D. *Inorg. Syn.* **1963,** *12,* 193.
(6) Epperson, E. R.; Horner, S. M.; Knox, K.; Tyree, S. Y. *Inorg. Syn.* **1963,** *7,* 163.
(7) Pouts, A. W.; Lyus, M. L. *J. Electron Spectrosc. Relat. Phenom.* **1978,** *13,* 305.
(8) Slater, J. C. "Quantum Theory of Molecules and Solids. The Self-Consistent Field for Molecules and Solids," Vol. 4; McGraw-Hill: New York, 1974.
(9) Johnson, K. H. *Annu. Rev. Phys. Chem.* **1975,** *26,* 39.
(10) Johnson, K. H.; Norman, J. G. Jr.; Connolly, J. W. D. "Computational Methods for Large Molecules and Localized States in Solids"; Plenum Press: New York, 1972.
(11) Johnson, K. H. *Adv. Quantum Chem.* **1973,** *7,* 143.
(12) Wood, J. H.; Boring, M. A. *Phys. Rev. B* **1978,** *18,* 2701.
(13) Cook, M. Harvard University. Bursten, B. E.; Stanley, G. G. Texas A&M University, 1979.
(14) Bertrand, J. A.; Cotton, F. A.; Dollase, W. A. *Inorg. Chem.* **1963,** *2,* 1166.
(15) Cotton, F. A.; Lippard, S. J. *Inorg. Chem.* **1965,** *4,* 50.
(16) Schwarz, K. *Phys. Rev. B* **1972,** *5,* 2466.
(17) Schwarz, K. *Theor. Chim. Acta* **1974,** *34,* 225.
(18) Herman, F.; Skillman, S. "Atomic Structure Calculations"; Prentice-Hall: Englewood Cliffs, N.J., 1963.
(19) Norman, J. G., Jr. *Mol. Phys.* **1976,** *31,* 1191.
(20) Watson, R. E. *Phys. Rev.* **1958,** *111,* 1108.
(21) Hall, M. B.; Fenske, R. F. *Inorg. Chem.* **1972,** *11,* 768.
(22) Bursten, B. E.; Jensen, J. R.; Fenske, R. F. *J. Chem. Phys.* **1978,** *68,* 3320.
(23) Bursten, B. E.; Fenske, R. F. *J. Chem. Phys.* **1977,** *67,* 3138.
(24) See paragraph at end of paper regarding supplementary material.
(25) Band intensities were corrected to account for the analyzer response by dividing the measured band areas by the kinetic energy of the electrons.
(26) Goldman, A.; Tejeda, J.; Shevchik, N. J.; Cardona, M. *Phys. Rev. B* **1974,** *10,* 4388.
(27) Berkowitz, J. *J. Chem. Phys.* **1974,** *61,* 407.
(28) Tejeda, J.; Braun, W.; Goldman, A.; Cardona, M. *J. Electron Spectrosc. Relat. Phenom.* **1974,** *5,* 583.
(29) Egdell, R. G.; Orchard, A. F. *J. Electron Spectrosc. Relat. Phenom.* **1978,** *14,* 277.
(30) Cotton, F. A.; Stanley, G. G. *Chem. Phys. Lett.* **1978,** *58,* 450.
(31) Mulliken, R. S. *J. Chem. Phys.* **1955,** *23,* 1833.
(32) Mortola, A. P.; Moskowitz, J. W.; Rösch, N.; Cowman, C. D.; Gray, H. B. *Chem. Phys. Lett.* **1975,** *32,* 283.
(33) Trogler, W. C.; Ellis, D. E.; Berkowitz, J. *J. Am. Chem. Soc.,* **1979,** *101,* 5896.
(34) Bursten, B. E.; Cotton, F. A.; Fanwick, P. E.; Stanley, G. G., in preparation.
(35) It is noted that there are kinks in the orbital contour plots at the intersections of the atomic spheres. These are due to the imperfect matching conditions imposed by the use of overlapping atomic spheres. They do not affect the orbital energetics or characters (cf. Herman, F.; Williams, A. R.; Johnson, K. H. *J. Chem. Phys.* **1974,** *61,* 3508).
(36) Averill, F. W.; Ellis, D. E. *J. Chem. Phys.* **1973,** *59,* 6412.
(37) Ellis, D. E. *J. Chem. Phys.* **1976,** *65,* 3629.
(38) In our Xα-SW calculations on $Mo_2(CH_2PH_2CH_2)_4$ and Cr_2(hydroxypyridine)$_4$ the ligand-based MOs were calculated to be ~2 eV too high in energy relative to the metal-based levels, although the level characters and respective metal–metal and ligand–ligand spacings appear to be qualitatively correct (unpublished results).
(39) Cotton, F. A.; Wilkinson, G. "Advanced Inorganic Chemistry", 3rd ed.; Wiley: New York, 1972; pp 979–980.
(40) Cotton, F. A. *Chem. Soc. Rev.* **1975,** *4,* 27.
(41) The 11e′ MO is actually a mixture of the Re–Re bonding seen in the 7e′ level and antibonding in the 8e′, yielding an orbital which is Re–Re nonbonding.
(42) Penfold, B. R.; Robinson, W. T. *Inorg. Chem.* **1966,** *5,* 1758.
(43) Elder, M.; Penfold, B. R. *Inorg. Chem.* **1966,** *5,* 1763.
(44) Bennett, M. J.; Cotton, F. A.; Foxman, B. M. *Inorg. Chem.* **1968,** *7,* 1563.
(45) Cotton, F. A.; Mague, J. T. *Inorg. Chem.* **1964,** *3,* 1094.
(46) Cotton, F. A.; Walton, R. A. *Inorg. Chem.* **1966,** *5,* 1802.
(47) Tisley, D. G.; Walton, R. A. *Inorg. Chem.* **1973,** *12,* 373.

Luminescent Photoelectrochemical Cells. 2. Doped Cadmium Sulfide Photoelectrodes as Probes of Excited-State Processes Which Influence Optical to Electrical Energy Conversion

Bradley R. Karas and Arthur B. Ellis*

Contribution from the Department of Chemistry, University of Wisconsin—Madison, Madison, Wisconsin 53706. *Received June 27, 1979*

Abstract: The use of n-type, Te- and Ag-doped CdS (5–1000 ppm CdS:Te, 10 ppm CdS:Ag) as electrodes in photoelectrochemical cells (PECs) employing (poly)chalcogenide electrolytes is described. Both polycrystalline and single-crystal (100 ppm CdS:Te) samples resemble undoped CdS in their ability to sustain the conversion of ultraband gap (~2.4 eV; $\lambda \lesssim 500$ nm) light into electricity with up to ~7% monochromatic efficiency. The doped electrodes serve as photoanodes for the oxidation of (poly)chalcogenide species. While serving as PEC electrodes, CdS:Te and CdS:Ag emit (λ_{max} ~600–700 nm) with ~0.01–1% efficiency. The origin and spatial character (global emission from local excitation) of the emission are discussed in terms of the measured absorption, emission, excitation, and photoaction (photocurrent vs. λ) spectra. We find that most PEC parameters including sustained operation only perturb the emission intensity, not its spectral distribution. Thus, the spectral distribution (540–800 nm) is found to be temperature dependent, but insensitive to the presence and composition of (poly)chalcogenide electrolytes, the excitation wavelength and intensity (457.9–514.5 nm; $\lesssim 30$ mW/cm^2), and the electrode potential. The emission intensity dependence on potential is striking: increasingly negative potentials lead to emission intensity increases of ~15–1200% between −0.3 V vs. SCE and the onset of cathodic current with ultraband gap excitation. The percentage increases correlate best with the maximum quantum efficiency for electron flow in the external circuit. Emission from band gap edge 514.5-nm excitation is more intense but far less sensitive to potential, displaying changes of at most a few percent. These effects are observed over a wide range of intensities. They are readily interpreted in terms of competition among excited-state deactivation routes in conjunction with the photoelectrochemical band bending model. The energetics of interfacial electron transfer are shown by open-circuit photopotential measurements to be comparable for undoped CdS and 100 ppm CdS:Te. Results bearing on the use of luminescent CdS:Te and CdS:Ag to probe electrode surface quality are also discussed.

Introduction

The use of photoelectrochemical cells (PECs) to mediate the direct conversion of optical energy to electricity is receiving widespread attention.[1] Typical PECs consist of an n-type semiconductor photoanode, a counterelectrode, and the electrolyte. The key elements are the semiconductor, which functions in the dual roles of photoreceptor and electrode, and

0002-7863/80/1502-0968$01.00/0

Scheme I

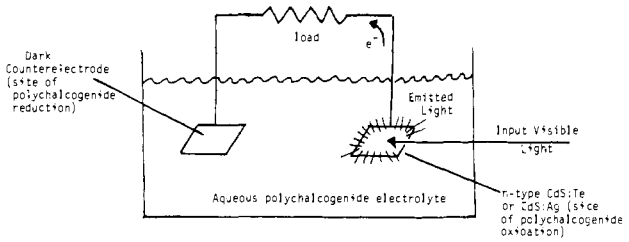

the electrolyte, which must possess the important feature of inhibiting the photocorrosion of the semiconductor. A variety of PECs have now been constructed using these principles and the goal of researchers in the field is generally to optimize the efficiency and longevity of such devices.

We feel that a promising avenue to optimizing efficiency involves characterization of the excited-state processes governing the semiconductor electrode. Deactivation of the excited electrode to produce photocurrent and, hence, electricity is only one of several decay paths available. We recently reported that luminescent Te-doped and Ag-doped CdS (CdS:Te, CdS:Ag) may be advantageously used to probe deactivation processes which defeat the production of electricity.[2,3] The methodology employed is to find materials which mimic the properties of efficient PECs while simultaneously exhibiting luminescence.

We have found that n-type CdS:Te and CdS:Ag meet these criteria and may be incorporated into the PEC shown in Scheme I. Analogous PECs based on undoped CdS have been studied extensively.[4] Direct conversion of optical energy to electricity in the CdS-based PEC results from oxidation of electrolyte polychalcogenide species at the photoanode and their simultaneous reduction at the counterelectrode. This sequence of reactions minimizes change in both the electrolyte and the electrode, since the polychalcogenide oxidation competitively precludes the process of photoanodic dissolution:

$$CdS \xrightarrow{h\nu} Cd^{2+} + S + 2e^- \qquad (1)$$

Both CdS:Te and CdS:Ag share these properties of undoped CdS, but they also emit at room temperature while serving as photoelectrodes. By assembling the PEC in the sample chamber of an emission spectrometer, both current and luminescence may be monitored simultaneously.

The physics of photoelectrochemistry has been elegantly described by Gerischer.[5] Interpretation of the role of emission in the PEC is best made with reference to Figure 1 where a photogenerated electron–hole (e^-–h^+) pair represents the semiconductor excited state. Deactivation routes available to the excited state are influenced by band bending. This potential gradient assists the separation of e^-–h^+ pairs leading to photocurrent. Two Faradaic processes have been identified: photocorrosion involving rate constant k_d and thermodynamic potential E_D, and energy conversion with rate constant k_x and potential E_{redox}.[6] Photocurrent is thus a measure of $(k_x + k_d)$, but chemical means must be used to distinguish the contribution of each process. The role of stabilizing electrolytes has been to maximize k_x.

Competing with nonradiative e^-–h^+ separation is e^-–h^+ recombination. Of course, this process defeats the conversion to electricity, since no current will pass in the external circuit. We may differentiate between radiative and nonradiative recombination with rate constants k_r and k_{nr}, respectively. Nonradiative recombination results in heat via lattice vibration; radiative recombination is the source of luminescence.

In the context of the PEC, we ultimately wish to characterize the various k_i shown in Figure 1. Measurement of photocurrent provides an experimental handle on e^-–h^+ separation pro-

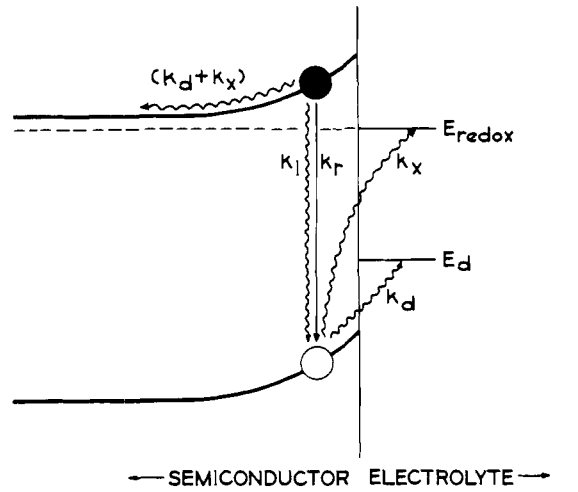

Figure 1. Excited-state deactivation pathways of the semiconductor electrode. Wavy arrows signify nonradiative decay routes: k_{nr}, k_d, and k_x correspond to electron (filled circle)–hole (open circle) recombination leading to heat, electron–hole separation leading to photoanodic decomposition, and electron–hole separation leading to electrolyte redox reactions, respectively. The straight arrow and k_r correspond to radiative recombination, the source of luminescence. E_d is the thermodynamic potential for anodic decomposition; E_{redox} is the potential of the electrolyte redox couple. Intraband gap states and defects which might play a role in the various deactivation routes have been omitted for simplicity.

cesses, and either luminescence or photothermal spectroscopy[7] can be used to probe e^-–h^+ recombination. The simultaneous measurement of separation *and* recombination affords a direct determination of the role of the various PEC parameters (electrode potential, electrolyte, incident wavelength and intensity, temperature) in partitioning input energy among the several excited state deactivation paths.

The value of such information is twofold. First, it permits the adjustment of experimental PEC parameters so as to maximize optical to electrical energy conversion by minimizing e^-–h^+ recombination processes. These parameters can also be adjusted to maximize luminescence for other kinds of energy conversion based, for example, on energy transfer across the semiconductor–electrolyte interface. Second, the data obtained should allow an assessment of the band bending model used to describe photoelectrochemical events.

Prior to the present work with doped CdS, the only PEC photoluminescence studies of which we are aware are those by Memming and Beckmann with n- and p-GaP[8] and by Petermann et al. with ZnO, ZnO:In, and ZnO:Cu,[9] all in aqueous acidic media. Although only p-GaP is photoinert under these conditions, correlations between emission and photocurrent can be drawn from these studies as will be discussed later. We demonstrate herein that the emissive and electrochemical properties of stabilized CdS:Te- and CdS:Ag-based PECs are profitably described in terms of the band bending model. Furthermore, the existence of multiple deactivation routes provides a powerful tool for examining the interplay of electron-hole separation and recombination processes as a function of various PEC parameters.

Results and Discussion

Characterization of CdS:Te- and CdS:Ag-based PECs differs from the undoped CdS-based PEC in the incorporation of luminescence measurements. This is achieved by assembling a PEC like that shown in Scheme I (photoelectrode, Pt foil counterelectrode, and SCE reference electrode) in the compartment of an emission spectrometer. The n-type photoanode is positioned at ~45° to both the exciting Ar ion laser beam and the emission detection optics so that principally front

Table I. Stability of n-CdS:Te and n-CdS:Ag Photoelectrodes in Aqueous Polychalcogenide Electrolytes

expt	electrode[a]	electrolyte[c]	electrode, mol × 10^4 [d] before	electrode, mol × 10^4 [d] after	electrons,[e] mol × 10^4	av i,[f] mA	time, h	V_{appl}[g]	source[h]
1	CdS:Te 5 ppm	S_n^{2-}	2.28	2.31	7.72	0.143	144.4	−0.05	Xe
2	CdS:Te 100 ppm	S_n^{2-}	2.41	2.39	6.49	0.122	143.2	−0.05	Xe
3	CdS:Te 1000 ppm	S_n^{2-}	2.69	2.67	6.95	0.084	222.4	−0.05	Xe
4	CdS:Te[b] 100 ppm	S_n^{2-}	6.67	6.59	12.9	0.192	181.0	−0.05	Xe
5	CdS:Te[b] 100 ppm	S_n^{2-}	10.7	10.5	3.6	0.749[i]	12.9[i]	−0.775	Ar^+
6	CdS:Ag 10 ppm	S_n^{2-}	1.49	1.47	5.24	0.102	138.1	−0.05	Xe
7	CdS:Te[b] 100 ppm	Te_n^{2-}	10.49	10.46	50.4	2.26	59.8	−0.05	Hg
8	CdS:Te[b] 100 ppm	Se_n^{2-}	8.11	7.95	100	3.74	71.6	−0.05	Hg
9	CdS:Te 1000 ppm	S_n^{2-}	0.847	0.820	1.73	0.069	67.2	−0.05	Hg
10	CdS:Te 100 ppm	S_n^{2-}	136.7	136.7	5.17	0.066	210.0	−0.05	Hg
11	CdS:Ag 10 ppm	S_n^{2-}	1.87	1.70	5.14	0.117	117.8	−0.05	Hg
12	CdS:Ag 10 ppm	Te_n^{2-}	1.27	1.26	1.31	0.086	40.8	0.00	Xe
13	CdS:Te 100 ppm	Te_n^{2-}	9.36	8.75	3.96	0.259	41.0	0.00	Xe

[a] Doped CdS polycrystalline (see footnote *b*) samples used as the photoanode in a PEC such as sketched in Scheme I or as the working electrode in a three-electrode potentiostatic PEC. Electrode resistivities are given in the Experimental Section; generally ~0.25–1.00 cm^2 of surface area is exposed to the electrolyte. Oxidation at the photoelectrode is that of (poly)chalcogenide species. Electrodes in experiments 1–8 are etched with Br_2/MeOH, those in experiments 9–13 with HCl. [b] Single-crystal electrodes of ~2 Ω cm resistivity whose irradiated face is perpendicular to the *c* axis. The more specular 0001 face was irradiated. [c] The polysulfide electrolyte, S_n^{2-}, is 1 M OH^-/1 M S^{2-}/1 M S except for experiments 6 and 9–11, where it is 1 M OH^-/1 M S^{2-}/0.2 M S. Experiments were N_2 purged and interrupted every 2 days to renew the electrolyte. Diselenide electrolyte, Se_n^{2-}, is 5 M OH^-/0.117 M Se^{2-}/0.001 M Se_2^{2-}; ditelluride electrolyte, Te_n^{2-}, is 5 M OH^-/0.083 M Te^{2-}/0.014 M Te_2^{2-} for experiment 7 and 5 M OH^-/0.05 M Te^{2-}/0.01 M Te_2^{2-} for experiments 12 and 13. These solutions were N_2 purged and magnetically stirred during the experiments. [d] Moles of crystal determined before and after the experiment by weight. In some cases the crystal chipped while being demounted and could not be fully recovered. [e] Moles of electrons passed during the experiment as determined by integrating photocurrent vs. time plots. [f] Average current during experiment. Current densities are roughly a factor of 1–4 larger (mA/cm^2). [g] Applied potential from a power supply serving as the load in Scheme I; the photoelectrode was connected to the negative terminal of the power supply. For experiment 5 a potentiostatic three-electrode geometry was employed with CdS:Te at −0.775 V vs. SCE. [h] Xe is a 150-W unfiltered Xe lamp; Ar^+ is the 496.5-nm line of an Ar laser; Hg is a 200-W super-high-pressure Osram lamp in a Bausch and Lomb housing whose output was monochromatized between 425 and 500 nm for maximum photocurrent. [i] Experiment described in Figures 2 and 3. Table entries do not include photocurrent passed or time elapsed during *iLV* and out-of-circuit emission spectral measurements.

surface emission is detected. Uniform illumination of the electrode surface is facilitated by 10× expansion of the laser beam. The electrodes, polycrystalline 5, 50, 100, and 1000 ppm CdS:Te, 10 ppm CdS:Ag, and single-crystal 100 ppm CdS:Te were etched in Br_2/MeOH or HCl before use. Results related to the 100-ppm, single-crystal CdS:Te material are emphasized, since its growth and properties were the most reproducible.

In the sections below we present typical PEC measurements of electrochemical stability, absorption and photoaction spectra, current–voltage curves, and optical-to-electrical energy conversion efficiency. Perhaps not surprisingly, the doped and undoped CdS electrodes do not differ substantially with respect to these measurements. We also present the luminescent counterpart of these properties for the doped CdS electrodes: emissive stability, emission and excitation spectra, current–luminescence–voltage (*iLV*) curves, and measures of emissive efficiency. The principal conclusions are that both electrochemical and emissive stability obtain for CdS:Te and CdS:Ag electrodes in polychalcogenide electrolytes, and that, although the emission spectrum is insensitive to several PEC parameters, the emission intensity is dependent on excitation wavelength and intensity and on electrode potential. Both the emission spectrum and intensity are temperature dependent. In the final section we discuss the integration of luminescence into the excited-state deactivation scheme of Figure 1.

A. Electrochemical and Emissive Stability. Establishing stability is a critical first step in characterizing doped CdS-based PECs, since it defines the time scale over which other measurements can be made. We have examined five measures of stability: stoichiometry, electrode surface stability, evidence for electrolyte oxidation processes, and the temporal variation of photocurrent and emission.

1. Stoichiometric Data. The stoichiometric measure of stability simply consists of passing enough photocurrent through the external circuit to largely or completely decompose the electrode by eq 1. Table I indicates that in polysulfide, diselenide, or ditelluride electrolytes there is negligible decomposition by weight. In many instances complete electrode consumption would have been expected.

2. Surface Effects. Electrode surfaces before and after the stoichiometric experiments in Table I showed minimal surface damage in polychalcogenide electrolytes. We do find occasional blackening of the surface in sulfide media (1 M OH^-/1 M S^{2-}), particularly at current densities in excess of ~10 mA/cm^2. Surface analysis of the damaged region by Auger spectroscopy indicates a significant increase in oxygen content, leading us to believe that an oxide layer forms under these

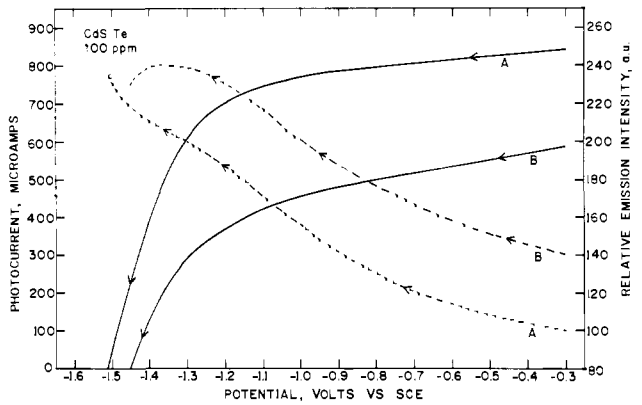

Figure 2. Photocurrent (solid lines, left-hand scale) and luminescence intensity (dashed lines, right-hand scale) monitored at 600 nm vs. potential for a single-crystal 100 ppm CdS:Te electrode in polysulfide (1 M OH^-/1 M S^{2-}/1 M S) electrolyte excited with ~7.5 mW of 496.5 nm using a beam-expanded Ar ion laser. This power is uncorrected for electrolyte absorbance and represents an upper limit. Curves labeled A were taken at the start of the experiment, those labeled B after 12 h of photoexcitation with the electrode at −0.775 V vs. SCE. During this period an average photocurrent of 700 μA (~2.5 mA/cm²) was passed. Emission intensity and photocurrent were recorded simultaneously (cf. Experimental Section and text) at a sweep rate of ~13 mV/s. The laser intensity was constant to ±5% for the duration of the experiment. E_{redox} was −0.74 V vs. SCE.

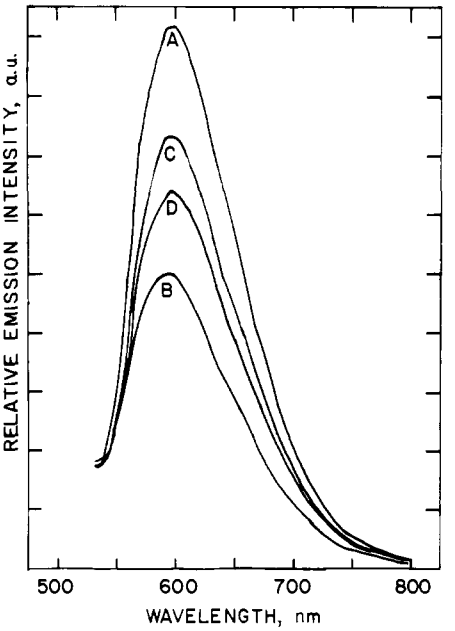

Figure 3. Uncorrected emission spectra for the experiment of Figure 2. Curves A and B are spectra taken at open circuit and −0.775 V vs. SCE, respectively, at the start of the experiment; curves C and D are out-of-circuit and in-circuit (−0.775 V vs. SCE) spectra taken after 12 h of continuous irradiation. A Corning 3-66 filter was used to eliminate the laser excitation peak and is responsible for the cutoff at the high-energy end of the spectra.

conditions. Our early experiments were carried out with HCl-etched electrodes which led to satisfactory stoichiometric data (Table I, experiments 9–13) but produced surfaces which were often darkened at high light intensities. The use of Br_2/MeOH as an etchant yields surfaces which are visibly more stable at comparable light intensities. Additionally, we obtain PEC properties which are both more reproducible and more akin to those of undoped CdS with the Br_2/MeOH etch. A possible explanation for the superiority of this etchant may lie in enhanced chemical reactivity with the lattice dopants.

The question of surface stability is quite significant, since there is now evidence that surface reorganization processes do occur even in PECs deemed relatively stable.[10-12] One mechanism involves exchange of lattice atoms; for example, substitution of S for Se in CdSe electrodes used in polysulfide electrolytes has been demonstrated.[11,12] Although a common species in the electrolyte and electrode would seem to obviate this possibility, a recent study of CdS electrodes in polysulfide electrolyte indicates that surface reorganization may still be occurring.[10] A second surface alteration mechanism which is germane to CdS:Te electrodes is based on the instability of CdTe to photoanodic decomposition in (poly)sulfide electrolytes.[4c] Some of the samples were examined (electron microprobe, Auger) before and after sustained PEC operation. Although we saw no evidence of Te, we cannot rule out this or lattice exchange processes entirely.

3. Competitive Oxidation. We also sought direct evidence for oxidation of the (poly)chalcogenide electrolyte species. Sustained PEC operation with single-crystal 100-ppm CdS:Te in transparent 1 M OH^-/1 M S^{2-}, 5 M OH^-/0.12 M Se^{2-}, and 5 M OH^-/0.11 M Te^{2-} results in yellow polysulfide, yellow-brown diselenide, and purple ditelluride solutions, respectively. At high light intensities in quiescent (di)telluride electrolytes, the orange CdS:Te emission is muted by a layer of metallic Te and/or purple Te_2^{2-}. Vigorous stirring removes this layer as purple Te_2^{2-} with recovery of emission intensity. Similar electrochemistry based on yellow-brown diselenide production in (di)selenide solutions has been observed with undoped CdS.[4c] The corresponding effect in polysulfide electrolytes is masked by the mutual orange color of the electrolyte and emission. Though not quantitative, these results as a body are consistent with efficient oxidation of electrolyte species.

4. Photocurrent and Emissive Stability. The most important measure of stability from the standpoint of sustained PEC operation is the time dependence of photocurrent and luminescence. Like undoped CdS, both CdS:Te and CdS:Ag suffer rapid declines in photocurrent in 1 M OH^- electrolyte where decomposition via eq 1 occurs. The S so produced also quenches the luminescence. Electrolytes containing (poly)chalcogenide ions stabilize the photocurrents of doped CdS anodes, and we find that the electrodes still emit at the conclusion of the stoichiometric experiments in Table I. We have attempted to put photocurrent and emissive stability on a more quantitative footing by simultaneously monitoring both over a 12-h period for a single-crystal 100-ppm CdS:Te electrode excited at 496.5 nm in 1 M OH^-/1 M S^{2-}/1 M S electrolyte.

Presented in Figure 2 are current-luminescence-voltage curves for the aforementioned PEC at zero time and after 12 h of photolysis (curves A and B, respectively). The maximum photocurrent declines slowly and monotonically over this period in a manner not unlike that reported for undoped CdS-based PECs.[4b,c] We also monitored the emission spectrum in circuit at −0.775 V vs. SCE, the potential at which current was passed during the experiment, and at open circuit, Figure 3. While the spectral distribution of emitted light is constant throughout, we see a decline in the open-circuit emission intensity and an increase in the in-circuit emission intensity. The discrepancy between in- and out-of-circuit intensities will be more fully developed below, but for now we wish to emphasize that, for the relatively large current densities of 2.5 mA/cm², changes in photocurrent and emissive intensity are slow and the emission spectrum is preserved. Moreover, after a similar experiment with the same electrode lasting for 4 h, a satisfactory stoichiometry was obtained (Table I, experiment 5).

B. Optical Properties. The composite data of the preceding section make a strong case for electrochemical and emissive stability for CdS:Te- and CdS:Ag-based PECs in aqueous

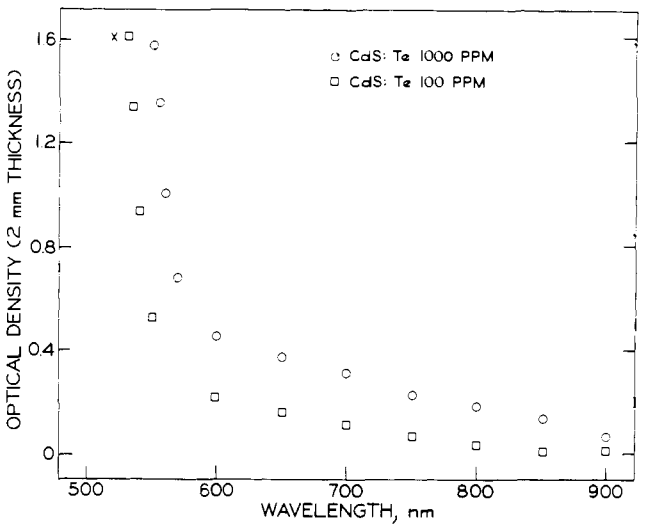

Figure 4. Optical density of polycrystalline 100 ppm CdS:Te (squares) and 1000 ppm CdS:Te (circles). Thicknesses are 2.0 and 2.2 mm, respectively, and samples have been polished with 1-μ alumina. The "x" is a literature value optical density of a 2-mm thick, undoped, polished CdS single crystal.[4b] Single-crystal 100 ppm CdS:Te gave an essentially identical absorption spectrum with that shown here for the polycrystalline material.

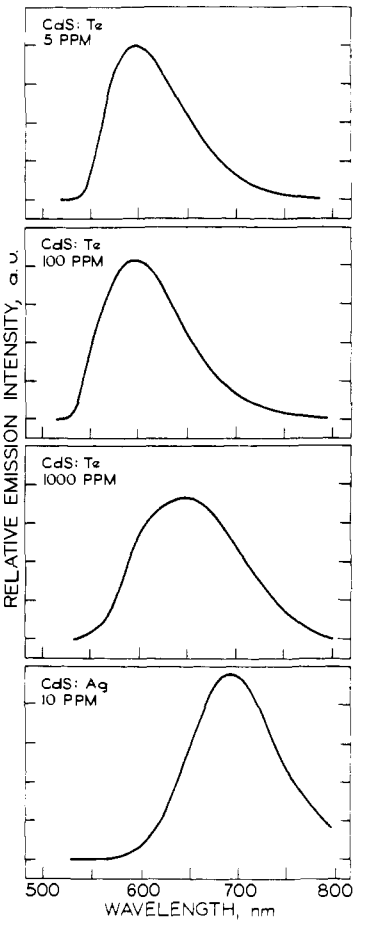

Figure 5. Typical 295 K uncorrected emission spectra of HCl-etched 5, 100, 1000 ppm CdS:Te and 10 ppm CdS:Ag. The CdS:Te samples were excited at 488.0 nm and the CdS:Ag sample at 514.5 nm. Etching with Br_2/MeOH gives essentially identical spectra.

polychalcogenide electrolytes and permit the determination of in situ optical properties. Because the electrodes luminesce, a complete characterization of these PECs demands emission and excitation spectra in addition to absorption and photoaction (photocurrent vs. λ) spectra. We also need to establish the extent to which the PEC and corresponding experimental parameters perturb these optical properties.

1. Absorption Spectra. The physical quantity which dominates optical interpretation is the band gap. Undoped CdS has a band gap of ~2.4 eV corresponding to an absorption onset of ~520 nm.[13] Doping CdS with Te or Ag results in obvious color changes, viz., undoped CdS is yellow, 5–100 ppm CdS:Te is orange, and 1000 ppm CdS:Te is orange-red; similarly, 10 ppm CdS:Ag is red and 100 ppm CdS:Ag is brown.

In Figure 4 we present absorption spectra of ~2-mm thick polycrystalline 100 and 1000 ppm CdS:Te samples. The single-crystal and polycrystalline 100 ppm CdS:Te yield identical spectra. A low-energy tail is seen to be responsible for the color differences. Comparison with a corresponding point from an undoped CdS absorption spectrum (the "x" in Figure 4) indicates that the tail red shifts with increasing Te concentration, an observation in accord with several literature reports.[14,15] Additionally, absorptivities calculated from Figure 4 are in approximate agreement with those measured by Moulton in the region of spectral overlap.[16] Our samples are too thick, however, to probe the band gap region.

Absorptivities, α, for undoped single crystal CdS have been measured at 295 K and are $\sim 10^5$ cm^{-1} at ultraband gap wavelengths ($\lambda \leq 500$ nm) and $\sim 10^3$–10^4 at 515 nm. A sample of single-crystal 1000 ppm CdS:Te examined by Moulton exhibits significantly greater absorption for $\lambda \geq 520$ nm than does CdS, but α is still $\sim 10^3$–10^4 at 515 nm, the high-energy limit of the measurement.[16] While the incorporation of small quantities of Te or Ag into the CdS lattice should not alter the band gap appreciably, the dopants do mask the band gap's exact position.

2. Emission Spectra and Mechanism. Crucial to an understanding of luminescent PECs are the origin and nature of the emitted light. Figure 5 presents the 295 K uncorrected emission spectra of the various polycrystalline samples employed in this study. Although the spectra shown are for HCl-etched samples, etching with Br_2/MeOH has no obvious effect on the spectral distribution nor does the single-crystal 100 ppm CdS:Te spectrum differ from its polycrystalline counterpart (cf. Figures 3 and 5). Note that, though the 5 and 100 ppm CdS:Te spectra look similar with maxima at ~600 nm, the 1000 ppm CdS:Te maximum has red shifted to ~650 nm, consistent with the red shift of its absorption tail relative to the more lightly doped samples. The maximum of the 10 ppm CdS:Ag emission is even further shifted to ~700 nm. Roessler has reported that the Te concentration, [Te], in CdS:Te may be estimated from λ_{max} and the full width at half maximum intensity, fwhm.[15] Although our emission spectra are uncorrected, the doping levels are in qualitative agreement with the literature trends.

The observation of emission maxima between ~2.06 and 1.95 eV implicates an intraband gap state. For CdS:Te Te is thought to substitute for S in the CdS lattice and, because of its lower electron affinity, to introduce a state ~0.2 eV above the valence band.[14-18] Holes trapped at Te sites may Coulombically bind an electron in or near the conduction band to form an exciton whose subsequent radiative recombination is the source of luminescence, Figure 6. Because Te is isoelectronic with S, it is only nominally a dopant and should not appreciably affect electrical properties such as resistivity, in accord with our observations. There are actually two emission bands reported in the literature for CdS:Te and their relative importance is a function of [Te]. At low [Te] (e.g., 100 ppm) the band at ~2.1 eV is observed and is believed due to an exciton bound at a single Te site. With increasing [Te] another band at ~1.7 eV begins to dominate the spectrum and is

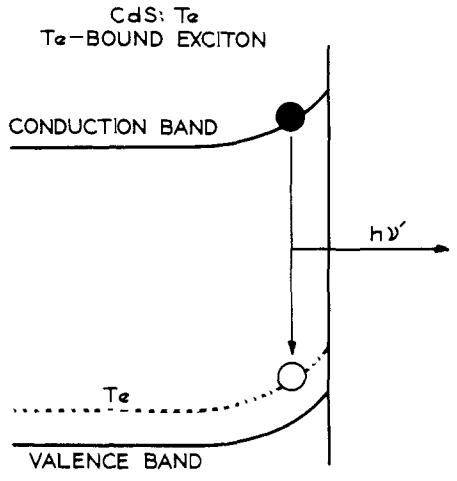

Figure 6. The origin of luminescence in CdS:Te. Te is an isoelectronic dopant which is believed to introduce an intraband gap state ~0.2 eV above the valence band. A hole (open circle) can be trapped at a Te site as shown and Coulombically bind an electron (filled circle) in or near the conduction band, forming an exciton. Radiative collapse of the exciton leads to the observed luminescence.

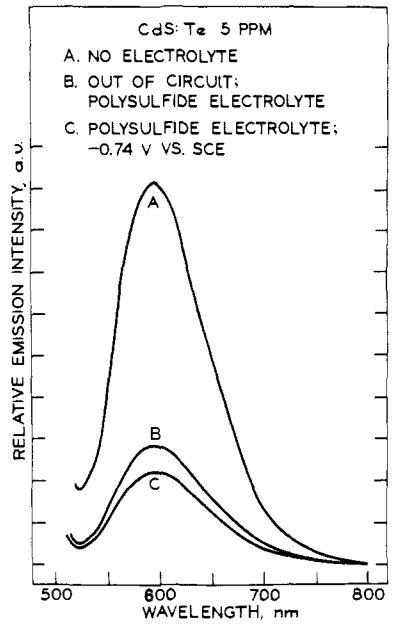

Figure 7. Uncorrected emission spectra of 5 ppm HCl-etched, polycrystalline CdS:Te in various environments but in a fixed geometry relative to the 488.0-nm laser excitation source and emission detection optics. For curve A no electrolyte was present; curves B and C were both taken with the electrode immersed in 1 M OH^-/1 M S^{2-}/1 M S polysulfide electrolyte, but out of circuit and in circuit at −0.74 V vs. SCE (E_{redox}), respectively. The sharp intensity drop from A to B and C is the result of electrolyte absorption; base line is not preserved at the high-energy end of the emission spectrum owing to overlap with the tail of the excitation line.

thought to arise from excitons trapped at several nearest-neighbor Te sites.[14-17] These 2.1- and 1.7-eV bands are the only ones observed at low temperatures (4.2 K) and represent exciton binding energies of ~0.2 and 0.4–0.6 eV, respectively.[14]

The energy of CdS:Ag emission is consistent with a mechanism differing from that of CdS:Te. However, the mechanism is complex; ambiguities are related to how Ag enters the lattice (interstitially or as a Cd substituent) and what role impurities play.[19]

Related to the question of mechanism is the geometric distribution of emission. The majority of our experiments with PECs have been carried out with uniform illumination of the entire exposed electrode surface, and we observe emission from all irradiated regions. However, irradiation with the unexpanded laser beam (2–3 mm diameter) results in emission from the irradiated and unirradiated regions, but most intensely from the former. We can offer at least three possible explanations for this phenomenon of global emission from local excitation: (1) Free excitons (a Coulombically bound valence band hole and conduction band electron) might migrate to and radiatively recombine at various Te trapping sites throughout the lattice. Estimates of diffusion lengths for free excitons in CdS:Te at 298 K are $<10^{-4}$ cm,[16] however, and render this an unlikely possibility. (2) Emission occurring from one bound exciton at a Te site might be repeatedly reabsorbed and reemitted. This, too, seems unlikely because of the low absorptivity of CdS:Te for the emitted frequencies. (3) Scattering or light trapping due to the high refractive index of the material is the most likely explanation, we feel. We should point out that emission is more uniform in the single-crystal material we have examined. Grain boundaries in our polycrystalline samples are 3–8 mm and on occasion we see abrupt cessation of emission at these boundaries. The boundary could be acting as a recombination trap if an exciton migration mechanism is involved or as an absorbing or reflecting surface in a scattering mechanism.

The extent to which emissive properties are perturbed by the PEC configuration is addressed by Figure 7. Curve A is the emission spectrum of 5 ppm polycrystalline CdS:Te excited at 488 nm in the absence of electrolyte. Without disturbing the experimental geometry, polysulfide electrolyte is added to the cell (curve B), and the electrode is then brought into circuit at −0.74 V vs. SCE (curve C). But for intensity all three curves are identical. The intensity drop from A to B is due to absorption by the orange electrolyte. A further decline in intensity from out of circuit to in circuit is typically observed with ultraband gap excitation (cf. Figures 2 and 3) and will be discussed below.

The insensitivity of the spectrum to potential is noteworthy. Variations in potential change the amount of band bending in the depletion region; for n-type semiconductors, negative bias reduces and positive bias augments band bending.[5] Because the emission spectrum involves intraband gap states, we feel that the energies of these states are bending in parallel with the valence and conduction bands, as shown in Figure 6. Insensitivity to potential has been exhibited by all of the electrodes in this study (both HCl- and Br_2/MeOH-etched). Also consistent with this model are the essentially identical emission spectra observed without electrolyte and with electrolytes of OH^-/X^{2-} and $OH^-/X^{2-}/X$ (X = S, Se, Te).

Like potential, the excitation wavelength only appears to affect the intensity of the emission spectrum. We find the low-resolution (bandwidth 5 nm) emission spectra at 295 K for the samples studied to be independent of Ar ion laser excitation lines from 457.9 to 514.5 nm at incident intensities $\lesssim$30 mW/cm^2; even at the higher intensities employed in some experiments (0.3 W/cm^2) we see no change in the spectrum. To summarize the results of this section, emission spectra of the doped CdS electrodes (~540–800 nm) are independent of the presence and composition of (poly)chalcogenide electrolytes, the electrode potential between ~−0.3 V vs. SCE and the onset of anodic photocurrent, and Ar ion laser excitation wavelengths and intensities (457.9–514.5 nm; $\lesssim$30 mW/cm^2).

3. Photoaction and Excitation Spectra. We have used the Ar ion laser lines to determine the dependence of photocurrent and emission intensity on wavelength. In Figure 8 we show such data for equal numbers of photons incident on a single-crystal

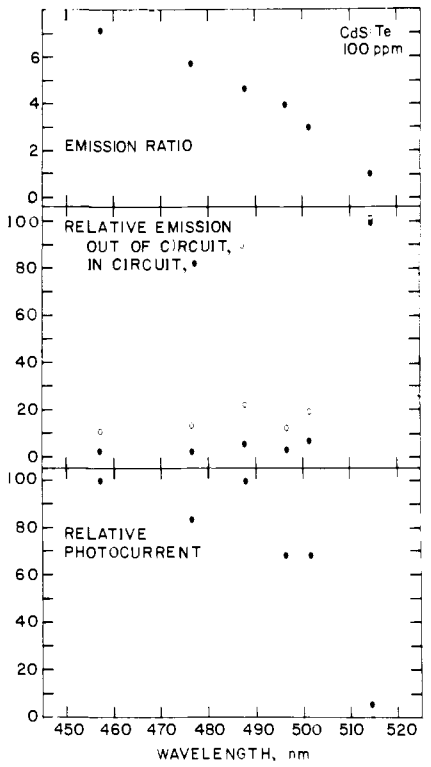

Figure 8. Bottom frame is a photoaction spectrum obtained by irradiating a single-crystal 100 ppm CdS:Te electrode in transparent 1 M OH^-/1 M S^{2-} electrolyte at −0.3 V vs. SCE with approximately equivalent numbers of photons at 514.5, 501.7, 496.5, 488.0, 476.5, and 457.9 nm with a beam expanded Ar ion laser. The photocurrent has been plotted relative to the value of 100 for 457.9-nm excitation. At each wavelength the relative emission intensity (middle frame) monitored at 600 nm was also measured, both in circuit at −0.3 V vs. SCE (filled circles) and out of circuit (open circles). A switch on the potentiostat permitted the PEC to be brought in or out of circuit without disturbing the cell geometry. Emission intensities are plotted relative to a value of 100 for 514.5-nm excitation. The top frame is the calculated ratio of open-circuit emission intensity to in-circuit emission intensity at each wavelength for the values given in the middle frame. We estimate the incident intensity to be 7.0×10^{-9} einstein/s·cm^2; the exposed electrode surface area is ~0.15 cm^2.

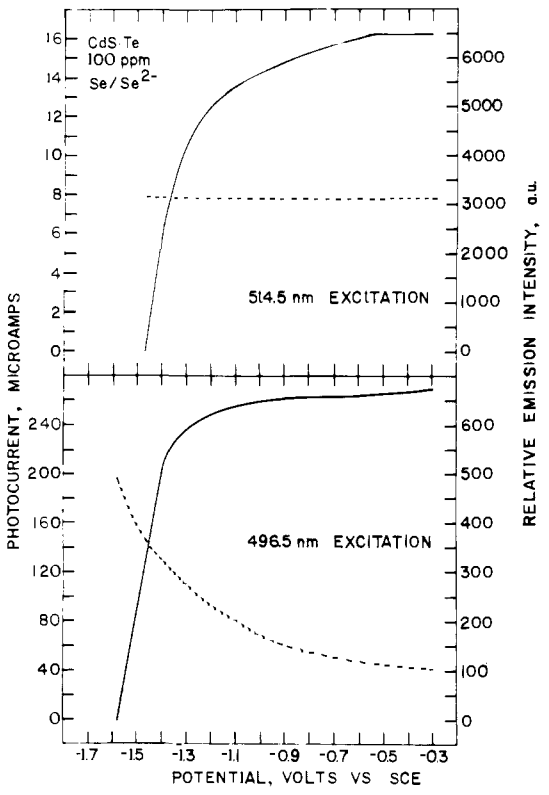

Figure 9. Photocurrent (solid line, left-hand scale) and emission intensity (dashed line, right-hand scale) monitored at 600 nm vs. potential for a CdS:Te 100 ppm single crystal electrode in 5 M OH^-/0.117 M Se^{2-}/0.001 M Se_2^{2-} electrolyte excited at 514.5 (top frame) and 496.5 nm (bottom frame). The Ar ion laser was beam expanded and irradiated the ~0.25-cm^2 exposed area of the electrode with ~0.8 mW at 514.5 nm and ~1 mW at 496.5 nm. These *iLV* curves were swept at ~13 mV/s. E_{redox} is −0.96 V vs. SCE.

100 ppm CdS:Te electrode in transparent 1 M OH^-/1 M S^{2-} electrolyte. The photocurrent (bottom frame) increases with decreasing wavelength with the largest increase occurring between 514.5 and 501.7 nm. We rationalize this by comparing the absorptivities at these wavelengths (vide supra) with the depletion region width of 10^{-4}–10^{-5} cm.[5] For $\lambda \lesssim 500$ nm e^-–h^+ pairs are formed within the region of maximum band bending where separation leading to photocurrent should be optimized. In contrast, a substantial fraction of 514.5-nm light will be absorbed outside the depletion region in a zone of negligible band bending.

Since emission represents a competing recombination process, we expected an inverse wavelength effect relative to the photoaction spectrum. The middle segment of Figure 8 illustrates this effect with the largest change again occurring between 501.7 and 514.5 nm. Both in-circuit (−0.3 V vs. SCE) and out-of-circuit intensities are displayed and, except at 514.5 nm, where they are almost equal, the latter is always greater. In fact, the ratio of the two, plotted in the figure's top frame, increases with decreasing wavelength. We offer an explanation in terms of e^-–h^+ pair balance. Photogenerated e^-–h^+ pairs may deactivate by any of the routes shown in Figure 1. As more pairs separate to yield photocurrent, fewer are left to recombine, radiatively or nonradiatively. With no photocurrent, the out-of-circuit condition, there is no competing separation process and the additional electron-hole pairs *must* recombine, some fraction of them radiatively. We thus expect the discrepancy between in- and out-of-circuit emission intensity to increase with Φ_x, the photocurrent quantum efficiency.

The excitation spectrum of Figure 8 was dependent on the sample in that ratios of ~2–30 for open circuit emission intensity excited at 514.5 vs. 501.7 nm were observed. We feel that this ratio may be a probe of surface quality. The presence of nonradiative recombination sites or traps in the surface region would preferentially quench emission based on the fraction of each wavelength absorbed in the region. In general, we see significantly less luminescence at ultraband gap wavelengths.

Complete excitation spectra for doped CdS:Te single crystals show a maximum near the band gap edge and correlations with the emission maxima have been established.[15,16] Excitation into the absorption tail of CdS:Te (Figure 4) does lead to emission and the intensity declines with increasing wavelength due to the progressive decline in sample optical density. We have observed emission from wavelengths as long as 540 nm.

Excitation into the absorption tail may directly create the Te-bound exciton.[15,16] Ultraband gap excitation can form the Te-bound exciton indirectly as noted above by the trapping at a Te site of a free exciton or a valence band hole. Inefficiencies in this process offer an alternative explanation for the declines in emissive efficiency with decreasing wavelength. In this sense it is important to recognize that the electron and hole of the emissive exciton may not have been the original photogenerated partners. The fungible nature of electrons and holes in conjunction with substantial thermal ionization energy at 295 K is believed responsible for the nonexponential emission decay times which have been observed. Typical lifetimes are on the order of several hundred nanoseconds.[14,17]

Table II. Intensity Dependence of Current-Luminescence-Voltage Properties[a]

electrolyte	λ_{ex}, nm	rel intensity[b]	rel photocurrent[c]	rel[d] Φ_r	rel[e] Φ_{r_0}	(Φ_{r_0}/Φ_r)[f]	OV, V vs. SCE[g]
OH^-/S^{2-}	514.5	1.0	1.0	1.0	1.0	1.0	−1.14
		2.4	2.4	2.6	2.6	1.0	−1.20
		9.6	9.6	11	11	1.0	−1.29
		28	28	33	33	1.0	−1.35
		88	85	100	98	1.0	−1.42
	501.7	1.0	1.0	1.0	1.0	2.8	−1.36
		2.8	3.1	3.3	3.5	3.0	−1.43
		4.3	4.2	4.7	4.9	3.0	−1.41
		6.6	7.2	8.3	8.7	3.0	−1.47
		29	30	38	44	3.3	−1.50
$OH^-/S^{2-}/S$	514.5	1.0	1.0	1.0	1.0	1.0	−1.04
		2.5	2.8	3.0	3.0	1.0	−1.09
		12	10	11.5	11	1.0	−1.16
		36	33	37	37	1.0	−1.24
		100	92	101	102	1.0	−1.31
	501.7	1.0	1.0	1.0	1.0	2.0	−1.20
		2.8	3.2	3.2	3.7	2.3	−1.29
		3.7	4.6	4.8	5.2	2.1	−1.32
		5.7	7.6	7.8	9.2	2.3	−1.37

[a] Single-crystal, 100 ppm CdS:Te used as the electrode in a PEC with the indicated electrolyte and excitation wavelength. All table entries represent data culled from a complete *iLV* curve swept at ~13 mV/s from −0.3 V vs. SCE to the onset of cathodic current. [b] Relative excitation intensities at the indicated wavelengths. The value 1.0 in both electrolytes is ~0.2 mW/cm² at 514.5 and ~0.4 mW/cm² at 501.7 nm, in sulfide electrolyte. Owing to the polysulfide absorption at 501.7 nm, we matched photocurrent at −0.3 V vs. SCE to the value in sulfide electrolyte. The intensity 1.0 at 501.7 nm is probably similar for the two electrolytes but not known for certain in polysulfide. Electrode area exposed to electrolyte is 0.25 cm². [c] Relative photocurrent at −0.3 V vs. SCE; photocurrent was saturated with respect to potential. [d] Relative emission intensity at −0.3 V vs. SCE monitored at 600 nm. [e] Relative open circuit emission intensity monitored at 600 nm. [f] Obtained by dividing the Φ_{r_0} value by the Φ_r value. Note that in general this value cannot be obtained by division of the preceding columns since those entries are relative to the incident intensity. [g] The onset voltage for photoanodic current in V vs. SCE. This is the potential at which Φ_{r_0} is measured.

C. Current-Luminescence-Voltage (*iLV*) Curves. A more meaningful presentation of the interrelationship between photocurrent and luminescence is provided by their complete potential dependence. We refer to these as *iLV* curves, since all three properties may be monitored concurrently. The insensitivity of the emission spectrum to potential (vide supra) provides the expedient of monitoring emission intensity by simply sitting at the emission band maximum.

1. General Features. In Figure 9 we present typical *iLV* data for a single-crystal 100 ppm CdS:Te electrode excited with comparable numbers of 496.5- and 514.5-nm photons in diselenide electrolyte. The photocurrent-voltage curves at these wavelengths are very similar to what would be observed for undoped CdS—an order of magnitude more photocurrent at the shorter wavelength and a diminution of photocurrent in passing to more negative potentials. The luminescence-potential behavior is quite different, however. At the ultraband gap wavelength of 496.5 nm, the emission intensity quintuples as the photocurrent declines to zero. With band gap edge 514.5-nm excitation the greater emission intensity is essentially constant over the excursion in potential. These results are correlated with the observations described in the preceding sections by noting that the onset of anodic photocurrent corresponds to open circuit.

Potential dependent emission intensity also obtains in polysulfide (Figure 2) and ditelluride[3d] electrolytes with ultraband gap excitation. The percentage increases in emission intensity between −0.3 V vs. SCE and the onset of cathodic current range from ~15 to 1200% for ultraband gap excitation. For band gap edge 514.5-nm excitation we have generally observed less than 5% variation over a similar potential range. We observe these effects independent of whether the voltage is swept, pulsed between the extreme voltages, or varied point by point. The variation of emission intensity is visibly obvious in a pulsed experiment. Successive multiple scans by any of the aforementioned methods are generally reproducible to within a few percent so long as cathodic current, possibly leading to electrode reduction,[6,20] is not passed.

The variation in magnitude of emission intensity with potential is intriguing, and we have adopted the ratio of open-circuit to in-circuit intensity (Φ_{r_0}/Φ_r) as a measure of the effect. The in-circuit intensity used is taken at a potential where photocurrent and emission intensity have reached limiting or saturated values. Values of Φ_{r_0}/Φ_r seem to correlate with the quantum efficiency for electron flow, Φ_x: the largest values of Φ_{r_0}/Φ_r ($\gtrsim 4$) which we have observed are with the single-crystal 100 ppm CdS:Te samples where $\Phi_x \geq 0.5$. Note, too, that, as Φ_x declines in Figures 2 and 3, so does Φ_{r_0}/Φ_r. The polycrystalline samples generally have smaller Φ_x with Φ_{r_0}/Φ_r values of $\lesssim 2.5$. With 514.5-nm excitation $\Phi_x \lesssim 0.1$ and here $0.95 \lesssim \Phi_{r_0}/\Phi_r \lesssim 1.05$. Also, both Φ_x and Φ_r exhibit their inverse changes in the same potential region as shown in Figures 2 and 9. The correspondence is not strictly adhered to, however, since we occasionally see a hump or plateau (Figure 2B) in the emission curves in sweeping toward negative potential. We do not know the origin of this anomaly, which appears most often at high incident light intensities or with electrodes exhibiting some surface damage; its further study is in progress.

One other noteworthy feature of the Φ_{r_0}/Φ_r ratio is that its magnitude is relatively independent of the (poly)chalcogenide electrolyte. We employed one single-crystal 100 ppm CdS:Te electrode in OH/S^{2-}, $OH^-/S^{2-}/S$, $OH^-/Se^{2-}/Se$, and $OH^-/Te^{2-}/Te$ and observed ratios of 2–5 in these electrolytes with 496.5-nm excitation. The experiments in sulfide and polysulfide electrolytes were conducted without disturbing the PEC geometry and the ratios were 3.0 and 2.5, respectively, with matched maximum photocurrents. In these experiments Φ_{r_0}/Φ_r was 1.00 with 514.5-nm excitation.

2. Intensity Effects. In Table II we present the *iLV* properties of a single-crystal 100 ppm CdS:Te electrode excited with 501.7- and 514.5-nm light at several intensities in sulfide and polysulfide electrolytes. To a first approximation the photocurrent, in-circuit (−0.3 V vs. SCE), and open-circuit emission intensities all increase linearly with incident light intensity. Linearity is sustained in both electrolytes over two orders of magnitude with 514.5-nm excitation; to within a few percent

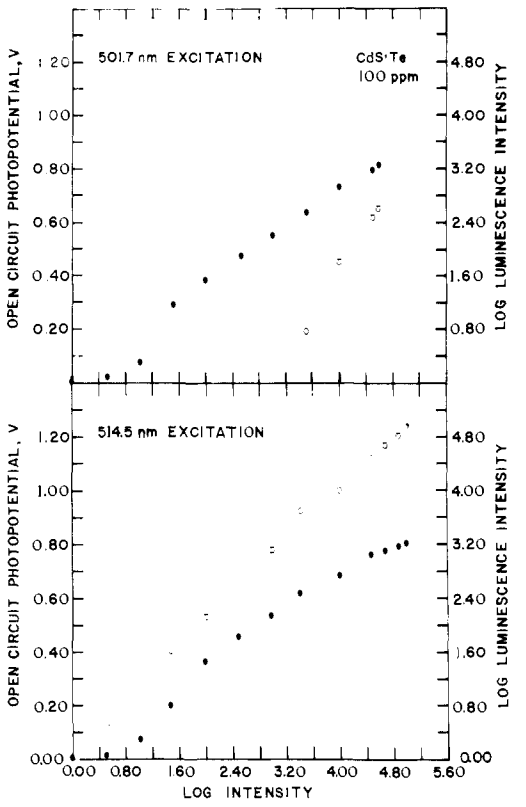

Figure 10. Open-circuit photopotentials (filled circles, left-hand scale) and log (emission intensity) (open circles, right-hand scale) monitored at 600 nm vs. log (intensity) for a 100-ppm single-crystal CdS:Te electrode in 1 M OH^-/1 M S^{2-}/1 M S polysulfide electrolyte excited with a beam expanded Ar ion laser at 501.7 (top frame) and 514.5 nm (bottom frame). The intensity was varied by laser power and an absorbing filter solution. The point 0.00 corresponds to ~0.7 μW at 514.5 nm on the ~5 × 5 mm electrode surface. The point 0.00 at 501.7 nm is more difficult to measure owing to unknown absorbance by the electrolyte, but is at most 0.3 μW. The emission intensity scale is identical for the two wavelengths, but the weaker emission from 501.7-nm excitation limited the range which could be examined. Photopotential and emission intensity were measured simultaneously in all cases. E_{redox} is −0.75 V vs. SCE.

Φ_{r_0}/Φ_r is unity in these experiments. With 501.7-nm excitation the weaker emission permitted only a factor of ~30 in intensity in sulfide electrolyte to be covered and only a factor of ~6 in polysulfide due to the solution's absorptivity at this wavelength. Both the photocurrent and the emission intensity (in and out of circuit) appeared somewhat superlinear. Superlinear and sublinear variations of emission intensity with incident intensity have been observed for "dry" CdS:Te crystals.[16]

D. Energetics. We have utilized open-circuit photopotential and optical to electrical energy conversion measurements to characterize the energetics of interfacial electron transfer for doped and undoped CdS electrodes. Additionally, measures of luminescence efficiency provide insight into the significance of emission in an energy balance sense as a decay route.

1. Open-Circuit Luminescence and Photopotential Measurements. The open-circuit photopotential, E_V, has been used extensively to place the conduction and valence band energies, E_{CB} and E_{VB}, respectively, relative to the electrolyte redox potential, E_{redox}.[4c,5a,21] In Figure 10 we present plots of E_V vs. log (intensity) for a single-crystal 100 ppm CdS:Te electrode obtained in polysulfide electrolyte with both 514.5- and 501.7-nm excitation (filled circles). Linearity is better with 501.7-nm excitation but saturation at $E_V \sim 850$ mV is more evident with high-intensity 514.5-nm light. Since E_{redox} is ~−0.75 V vs. SCE, we can set upper (positive) limits on the band positions as shown in Scheme II, assuming that the band

Scheme II

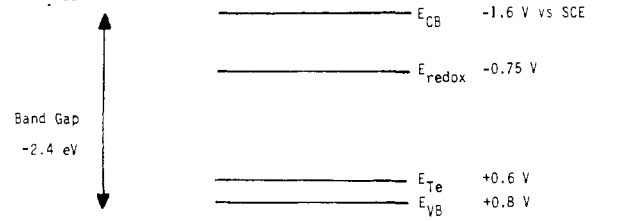

gap of CdS:Te is ~2.4 eV. The potentials of Scheme II are consistent with those reported for undoped CdS in polysulfide electrolyte.[4c,k]

While E_V was being measured, we simultaneously determined the relative emission intensity (open circles, Figure 10). The log–log plot reveals linearity with 514.5-nm excitation over five orders of magnitude in excitation intensity. Electrolyte absorption reduced the effective intensity range with 501.7-nm excitation, but superlinearity of emission intensity is evident over the region explored. The difference between the two wavelengths parallels the data in Table II with somewhat more pronounced superlinearity at 501.7 nm in Figure 10.

2. Optical to Electrical Energy Conversion. More evidence that the energetics of doped and undoped CdS-based PECs are similar is given by comparing their ability to convert optical energy into electricity. In Table III we offer criteria for a direct comparison of undoped CdS, single-crystal 100 ppm CdS:Te, and the various polycrystalline doped CdS electrodes. The data in Table III are culled from *iLV* curves like those in Figures 2 and 9. Although the polycrystalline doped CdS electrodes give somewhat lower values of η_{max}, single-crystal 100 ppm CdS:Te easily rivals undoped CdS in its 3–7% optical to electrical conversion efficiency. Significantly, the breakdown of η_{max} into output voltage and photocurrent (Φ_x at η_{max}) is quite similar. The low values of η_{max} for polycrystalline samples are primarily due to deficiencies in Φ_x. Grain boundaries are known to serve as e^-–h^+ recombination sites and are likely the source of these poorer efficiencies.[22]

3. Luminescence Efficiency. Ultimately, an overall energy balance is required to completely trace the partitioning of input energy by the semiconductor electrode excited state. In this section we offer estimates of emissive efficiency. There are two definitions of emissive efficiency which we find to be useful. One is (photons emitted)/(photons absorbed), the other is (energy emitted)/(energy absorbed). Interconversion of the definitions is based on the spectral distribution of emission.[23]

We have estimated the energy emitted by exploiting the spatially diffuse nature of the emitted light (vide supra) in conjunction with a flat wavelength response radiometer. By mounting the doped CdS electrodes edge on, both the front and back surfaces can be exposed to the electrolyte. The radiometer is placed behind the PEC as closely as possible to the electrode's emitting back surface. The light incident on the front surface is not detected owing to its complete absorption by the electrode. Correction for the fraction of the emitted light actually sampled leads to an estimate of 0.01–1% for the (energy emitted)/(energy absorbed) ratio. The value depends on the sample, excitation wavelength, and potential (vide supra).

We have made a second estimate based on finding an experimental parameter which would lead to greater radiative efficiency under comparable excitation conditions. In this manner an upper limit for Φ_r can be established. The CdS:Te literature indicates that a decrease in temperature leads to markedly brighter emission.[14-18] We have verified this observation with all of the samples studied. Figure 11 shows the spectral changes which occur upon cooling an unmounted, HCl-etched, 50-ppm, polycrystalline CdS:Te sample from 295 to 77 K. The spectrum has sharpened and a crude integration indicates a ~40-fold increase in photons emitted at the lower

Table III. Energy Conversion Characteristics in Aqueous Polysulfide Electrolyte[a]

property	undoped CdS-based PEC[b]	single-crystal 100 ppm CdS:Te-based PEC[b]	polycrystalline CdS:Te- and CdS:Ag-based PEC[b]
η_{max}[c]	3-8%	3-7%	0.2-5%
V at η_{max}[d]	0.3-0.5 V	0.3-0.5 V	0.3-0.4 V
Φ_x at η_{max}[e]	0.3-0.5	0.3-0.5	0.01-0.3
Φ_x max[f]	0.8-1.0	0.6-0.9	0.3-0.5
lum η[g]		0.01-1%	0.01-1%

[a] Measures of efficiency for the conversion of $\lesssim$10 mW/cm^2, ~500-nm monochromatic input optical energy to electricity and/or luminescence in aqueous polysulfide (1 M OH^-/1 M S^{2-}/1 M S) media. Listed values are representative. [b] The indicated n-type electrodes serve as photoanodes in a PEC like that shown in Scheme I or as the working electrode in a three-electrode potentiostatic geometry and are etched with Br_2/MeOH before use. Descriptions of the CdS:Te and CdS:Ag electrodes are given in the Experimental Section. Undoped CdS values are from ref 4b,c. [c] Maximum efficiency for the conversion of optical energy to electricity. These values are obtained from current-voltage curves like those in Figures 2 and 9 by maximizing the product of output voltage (cf. text and footnote *d*) and photocurrent, then dividing by input optical power. [d] Output voltage at maximum efficiency. The output voltage is the absolute value of the difference between the electrode potential on the current-voltage curve and E_{redox}. [e] Φ_x is the quantum yield for electron flow in the external circuit, measured here at the potential corresponding to maximum efficiency. [f] The maximum value of Φ_x, generally measured at ~0.4 V positive of E_{redox} where the photocurrent has saturated with respect to potential. [g] Efficiency for the conversion of optical energy to luminescence, defined here as (energy emitted)/(energy absorbed). A flat wavelength response radiometer is used to estimate the energy emitted; cf. Experimental Section and text. The indicated range encompasses variations in sample, excitation wavelength, and potential.

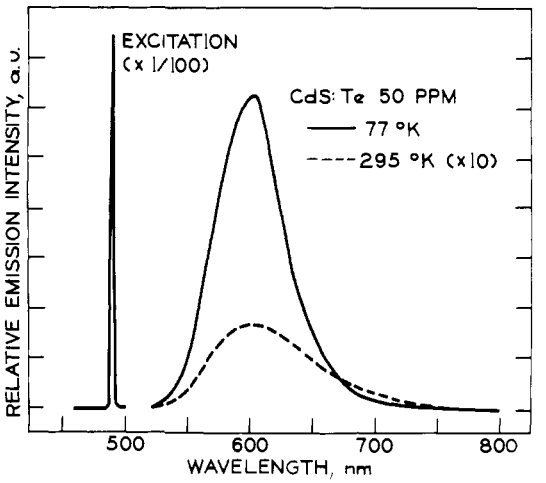

Figure 11. Uncorrected emission spectra of 50 ppm, HCl-etched, polycrystalline CdS:Te at 77 (solid line) and 295 K (dotted line; ten times scale expansion). The sample was excited with identical intensities of 488.0-nm light at the two temperatures without disturbing the experimental geometry.

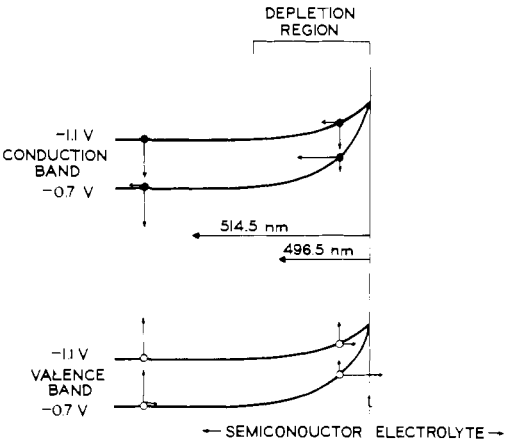

Figure 12. Representation of the joint effects of excitation wavelength and potential upon the quantum yields of electron flow in the external circuit, Φ_x (horizontal arrows), and luminescence, Φ_r (vertical arrows). The arrow lengths are roughly proportional to Φ_x and ~100Φ_r for the competing electron-hole separation and recombination processes, respectively. Conduction band electrons (filled circles) and valence band holes (open circles) have corresponding arrows to emphasize the pair nature of these processes. Intraband gap states have been omitted for simplicity. The potentials shown might be appropriate for (poly)sulfide electrolyte.

temperature. We generally see emission intensity increase by factors of ~4-80 from 295 to 77 K with 457.9-501.7-nm excitation. This yields an upper limit for 295 K emissive efficiency of 0.012-0.25, consistent with the 0.0001-0.01 range determined by the first method.

A qualification to this experiment arises from the known increase in CdS band gap with cooling;[13,16,24] the light is probably not absorbed in exactly the same location within the crystal at the two temperatures. This effect is quite dramatic with 514.5-nm light where at 77 K part of the laser beam is observed to pass through 1-mm thick samples; the other laser lines do not emerge at 77 K and none of the laser lines including 514.5 nm passes through at room temperature. We would expect the absorptivity difference to be least pronounced at 457.9 nm and in general our observed increases in emission on cooling are in agreement with those in the literature.[14-18]

E. Luminescence as a Probe of Recombination Processes. As the calculations in the preceding section indicate, luminescence is a minor contributor to the overall energy balance. Indeed, the bulk of input optical energy is ultimately converted to heat, since even under optimal conditions less than 10% of the input energy is recovered as electricity. The significance of emission rests, we believe, in monitoring the effects of PEC parameters on e^--h^+ recombination processes. All of our results regarding emission are readily compatible with the band bending model used to describe photoelectrochemical phenomena.

In Figure 12 we present a diagram which summarizes our observations in terms of band bending. The lengths of the horizontal arrows are roughly proportional to the photocurrent quantum efficiency, Φ_x; the lengths of vertical arrows reflect the magnitude of radiative quantum efficiency, ~100Φ_r. Filled circles in the conduction band and corresponding open circles in the valence band are pictured to emphasize the e^--h^+ pair nature of these separation and recombination processes. The band diagram is drawn at two potentials to accentuate the reduced band bending believed to occur with more negative potentials. Because ultraband gap photons (496.5 nm, e.g.) are absorbed in the depletion region of maximum band bending, separation and recombination processes should be quite sensitive to the electrode potential. As shown in Figure 12 and described in section C, increasingly negative potential leads to both reduced photocurrent and augmented emission intensity. Simply put, with reduced band bending there is less driving force for e^--h^+ separation and more likelihood for competing recombination. Since much of the 514.5-nm light is absorbed outside the depletion region in a zone of little band bending, we expect and observe more recombination to start with and less of an effect on that recombination as the potential is varied.

There is an alternative explanation for these observations invoking potential-dependent absorptivity, α. Electroabsorption measurements of undoped CdS reveal that variation in α with potential does occur and that $\Delta\alpha$ is wavelength dependent.[25] In general, $\Delta\alpha$ is less than 4×10^3 cm^{-1} and takes on both positive and negative values between ~520 and 470 nm for electric fields of 10^4–10^5 V/cm.[25] Although electroabsorption measurements have not to our knowledge been made on CdS:Te or CdS:Ag, we have several pieces of evidence which lead us to believe that the effect is small. First we obtained an *i–V* curve in sulfide electrolyte using a 100 ppm CdS:Te single-crystal electrode which was sufficiently thin to pass some of the exciting 514.5-nm beam. In monitoring the transmitted light with a radiometer, we saw negligible change in its intensity over the excursion in potential. Unfortunately, the increased absorptivity for ultraband gap photons precludes this experiment at those wavelengths. However, our second observation is the relative insensitivity of the *iLV* curves to ultraband gap excitation wavelengths. As mentioned above, electroabsorption data for undoped CdS show a great variation of $\Delta\alpha$ in this region. At this point, then, we feel that the variations in emission intensity and photocurrent which we observe with potential are due to alteration of band bending in fixed regions of the electrode.

The interpretation of emission in an operating PEC is greatly simplified by the insensitivity of the emission spectrum to the presence and composition of (poly)chalcogenide electrolytes, the (Ar ion laser) excitation wavelengths and intensity, and to applied potential. This latter property is particularly germane to the band bending model, since it implies that the energies of intraband gap states involved in the emissive transitions bend in parallel with the conduction and valence bands. It is especially gratifying to see these properties manifested in a variety of electrodes of different dopant composition and almost certainly possessing different emissive mechanisms. Of the experimental parameters investigated thus far, only temperature has significantly altered the spectral distribution of emitted light.

The best studied doped electrode, single-crystal 100 ppm CdS:Te, offers abundant evidence of closely mimicking undoped CdS. Its stabilization by (poly)chalcogenide electrolytes, *i–V* curves, energy conversion properties, and band positions as determined from open-circuit photopotentials are all strongly reminiscent of undoped CdS-based PECs. The doped CdS electrode offers insight into the redistribution of energy once photocurrent is removed as an excited-state deactivation route. It is clear that only a fraction of the electrical energy is recovered as radiative decay; the majority is funnelled into nonradiative recombination.

Besides energy redistribution, emission also offers information regarding surface quality. The condition of the electrode surface is a crucial feature of interfacial electron transfer. As Figure 2 shows, changes in both the emission intensity and photocurrent occur over time and are potential dependent. The emission intensity from 514.5-nm and ultraband gap excitation expressed as a ratio varies from sample to sample and seems to be related to surface quality—the efficiencies of decay routes are a function of optical penetration depth not only because of band bending, but also because the local environment in which e^-–h^+ pairs are formed may vary considerably due to lattice defects, traps, etc. We also see humps and plateaus in the luminescence portion of *iLV* curves under conditions where surface damage is more likely. Although our understanding of these phenomena is at a primitive stage, we feel that useful information regarding surface and near-surface conditions will eventually be provided by luminescence studies.

Related to this point is the comparison of polycrystalline and single-crystal samples. Direct comparisons have been made with 100 ppm CdS:Te. We find that the optical properties (absorption and emission spectra) are essentially identical, but that we invariably observe greater optical to electrical conversion efficiencies and larger ratios of Φ_{r_0}/Φ_r with the single-crystal material, although out-of-circuit emission intensities appear similar. We attribute the difference in properties to grain boundaries serving as recombination sites. Despite these differences polycrystalline materials are good approximations to the single-crystal electrodes and offer the considerable advantage of cost.

We feel that the most significant features of the present work are the clear correlation between PEC properties of a nonemitting and emitting electrode and the additional information realizable with the latter. Such studies need not be restricted to CdS. The competitive nature of photocurrent and emission has also been observed with p-GaP (Φ_{r_0}/Φ_r vas very small, probably due to low Φ_x),[8] ZnO,[9] and ZnO:Cu[9] electrodes. It is important to note that entirely different electrochemistry obtains in these systems: H_2 evolution at p-GaP and photocorrosion (to Zn^{2+} and O_2) with the ZnO electrodes. In the ZnO-based PECs a nearly mirror-image relationship between photocurrent and emission was observed. A derivation presented to account for it may be applicable to the stable doped CdS electrodes studied here at the highest values of Φ_x.

A complete model of the semiconductor excited state will ultimately require more exact knowledge of the optical penetration depth. An advantage of the p-GaP electrode over the doped CdS electrodes is that the indirect band gap of GaP[26] permits more reliable measurements of the penetration depth. Armed with this information, it should be possible to map the depletion region by obtaining *iLV* curves as a function of excitation wavelength. We emphasize that there is nothing intrinsically unusual about ZnO, ZnO:Cu, p-GaP, CdS:Te, or CdS:Ag. A considerable range of luminescence-inducing dopants is available for many electrodes commonly used in PECs,[27] making their deliberate introduction both feasible and desirable from the standpoint of characterizing the excited-state properties of the photoelectrode.

Experimental Section

Materials. Polycrystalline, n-type CdS:Te and CdS:Ag were obtained from Eagle-Picher Industries, Inc., Miami, Okla. The 5, 50, 100, and 1000 ppm CdS:Te disks had 18–20-mm radii, were 2–3 mm thick, and had resistivities (Hall method) of 0.69–1.12 Ω cm. CdS:Ag samples were purchased as ~1 g boules with resistivities of 2×10^3 to 2×10^6 Ω cm corresponding to 10–500 ppm, respectively. Grain boundaries in all of these melt-grown samples ranged from 3 to 8 mm. Plates of single-crystal 100 ppm CdS:Te, 10 × 10 × 1 mm and oriented with the 10 × 10 faces perpendicular to the *c* axis, were purchased from Cleveland Crystals, Inc., Cleveland, Ohio. This material was vapor grown and had a resistivity of 2.2 Ω cm (four point probe method). Values of [Te] and [Ag] are estimates based on starting quantities.

Electrode Preparation. The samples were cut into irregularly shaped pieces, ~0.25 cm^2 × 1 mm, etched in either concentrated HCl (30 s) followed by a distilled water rinse or in a 1:10 (v/v) Br_2/MeOH solution for 10–30 s. With the latter etchant samples were subsequently rinsed in distilled water, transferred to a beaker of MeOH, and placed in a Bransonic 220 ultrasonic cleaner for 10–12 min to remove residual Br. For single-crystal CdS:Te both etchants allow visual identification of the more specular 0001 "Cd"-rich and matte $000\bar{1}$ "S"-rich faces; the 0001 face was always exposed to the electrolyte.[28] Ohmic contact was made by rubbing Ga-In eutectic on one face of the etched samples. A Cu wire was inserted into a 5-mm o.d. glass tube and attached to the eutectic by conducting Ag epoxy. Clear epoxy resin was used to insulate all but the front surface of the electrode. Black epoxy was then spread over the cured clear epoxy to preclude undesired emission from the mounting materials.

Electrolytes. The preparation of (poly)sulfide electrolytes has been reported and differs only in the use of a N_2 rather than an Ar purge.[4b] Telluride (selenide) electrolytes were prepared as follows: 75 mL of an aqueous 5 M KOH solution was purged with N_2 and transferred

to both a 12 × 4 cm o.d. side-arm flask and to a 15 cm × 7 mm o.d. tube with a frit at the bottom. The tube had been pushed through a hole in a rubber stopper which fit the mouth of the flask and was lowered to immerse the frit in the N_2-blanketed solution. A Pt wire anode was placed in the electrolyte in the tube and a Te (Fisher 99.98%; 2.5 × 1 cm diameter) or Se (99%, source unknown, 4 × 2 × 1 cm) cathode was suspended by a Cu wire in the electrolyte in the flask. With rapid magnetic stirring, increasingly negative bias was applied to Te (Se) from an HP Model 6214A 12-V power supply until purple Te_2^{2-} or yellow-brown Se_2^{2-} was observed at the cathode. Solution volume was maintained by purging through a distilled-water reservoir. Aliquots of the flask solution were removed periodically and gravimetrically analyzed for Te (Se). The total Te (Se) concentration in the flask could be increased by simply adding Te (Se) powder. When the desired Te (Se) concentration was reached, the Te (Se) electrode was replaced with a Pt gauze (4 × 2 cm) electrode and the final reduction to colorless Te^{2-} (Se^{2-}) was performed. The concentration of Te_2^{2-} or Se_2^{2-} present was determined spectrophotometrically.[4c]

Cells. Experiments in (poly)sulfide electrolyte not involving emission measurements were performed in a 50 × 25 × 25 mm glass cell with a 3 × 1 cm Pt foil counterelectrode and, in some cases, an SCE. Experiments in (poly)sulfide requiring emission detection employ a "half-cell" made by cutting a 25-mm o.d. tube from its one flattened end in half along its axis for ~¾ of its length. A perpendicular cut was then made to the tube edge and microscope slides were cut to fit the holes and attached with epoxy. This half-cell geometry minimizes path length losses from electrolyte absorption when the PEC is in the compartment of the emission spectrometer, yet preserves enough room at the top of the cell for three electrodes and a N_2 purge. The more air-sensitive (di)telluride and (di)selenide electrolytes required a third cell which resembles a Lincoln log in shape and is made by indenting the center two-thirds (to half the 25-mm o.d.) of a 9-cm tube to which a side arm for N_2 purging has been attached. A small magnetic stirrer fits into the bottom of the cell and is driven by a motorized magnet located beneath the emission compartment; the semiconductor electrode and an SCE are inserted into the solution via the holes of a rubber stopper which fits the mouth of the cell, and a 5 cm × 1 mm diameter Pt wire counterelectrode is held against the side of the cell by the stopper which also serves as a vent. Solution volume is maintained by first passing the N_2 through a distilled-water reservoir.

Optical Measurements. Absorbance measurements were made on a Cary 14 spectrophotometer and emission measurements (200–800 nm) with an Aminco-Bowman spectrophotofluorometer equipped with a Hamamatsu R446S PMT for extended red response. Emission spectra are uncorrected and displayed on a HP 7004A x-y recorder; bandwidth is ~5 nm. Samples were always oriented at ~45° to both the excitation beam and detection optics to monitor front surface emission. Irradiation sources included an Osram SP200 super-high-pressure Hg lamp whose output was passed through a Bausch & Lomb 33-86-02 monochromator, a 150-W Xe lamp (Oriel Model 8500 Housing), and a Coherent Radiation CR-12 Ar ion laser. A 10× beam expander was used to enlarge the 2-3-mm diameter laser beam which was then translated upward by a periscope and brought into the emission spectrometer through a hole in the side of the emission compartment. The beam was masked by slits to fill the electrode surface. Laser intensity was attenuated by power adjustment, colored filters, and/or a 0.07 M $Na_2Cr_2O_7$ solution in a Precision Cells, Inc., variable path length (0.1–10 mm) cell. A Corning 3-66 filter was occasionally placed in front of the PMT to eliminate the laser excitation line. The laser intensity was measured with a Tektronix J16 radiometer equipped with a J6502 probe head (flat response ±7%, 450–950 nm) and/or a Scientech 362 power energy meter (flat response 250–35 000 nm). A quartz disk was used as a beam splitter during those experiments requiring continuous monitoring of intensity.

Stoichiometries. Etched crystals were weighed (±0.1 mg) prior to being mounted as electrodes. Long-term stability experiments in Sc_n^{2-} and Te_n^{2-} were conducted in the side-arm flask used for preparation of the electrolyte (one compartment experiment); a similar cell without the side arm but with N_2 purging was used for experiments in polysulfide electrolyte. This electrolyte was renewed every 48 h. The electrodes, electrolyte compositions, and light sources are given in Table I. The HP 6214A power supply was connected in series with the photoanode and the Pt foil counterelectrode; current was continuously recorded on a Varian 9176 strip-chart recorder as the potential drop across an in-series 10- or 100-Ω resistor. At the end of the experiment, the crystal was demounted and reweighed.

Surface Effects. The surfaces of several samples were examined after various etching procedures and after sustained PEC operation. An Applied Research Laboratories EMX electron microprobe (10 kV, 0.8 μA, 50-μ diameter beam) was used to analyze for Cd, S, Te (not detected), Cl, and Br. A Physical Electronics Model 548 spectrometer was used for Auger (3 kV, 30 μA, focused electron beam) and ESCA (Al Kα anode, 10 kV, 50 mA, both broad scan and high resolution) measurements of the same elements (Te not detected) plus oxygen.

Photocurrent and Emissive Stability. A single-crystal 100 ppm CdS:Te (Br_2/MeOH etch) electrode was positioned in the emission spectrometer and excited with the 496.5-nm laser line in polysulfide electrolyte with standard three-electrode geometry. The electrode potential was held at −0.775 V vs. SCE by a PAR 173 potentiostat/galvanostat and current (PAR 176 I/E converter) was continuously measured on the Varian recorder. At the beginning of the experiment and every hour for a total of 12 h, the iLV curve (vide infra) was recorded as well as the emission spectrum, both out of circuit and in circuit at −0.775 V vs. SCE. Throughout the experiment, the laser output was continuously monitored by splitting part of the beam into the Scientech power meter whose output was recorded on a Heath Model EU-205-11 strip-chart recorder.

Effects of PEC Parameters on Emission. Photoelectrodes were positioned in an empty cell in the emission spectrometer. The counterelectrode and SCE were then positioned and all electrodes were connected to the potentiostat. The emission spectrum (540–800 nm) was recorded, repeated after (poly)sulfide electrolyte was added to the cell (out of circuit), and repeated a third time after bringing the cell into circuit with a switch on the potentiostat. This sequence or parts thereof could be repeated with various laser excitation lines.

Photoaction, Excitation Spectra. Emission intensity at 600 nm was monitored from a single-crystal 100 ppm CdS:Te electrode in transparent 1 M OH^-/1 M S^{2-} electrolyte (standard three-electrode geometry). The electrode was excited sequentially with six laser lines from 457.9 to 514.5 nm such that the einsteins/s at each wavelength was about the same as determined by splitting part of the laser beam into the Tektronix radiometer. Filters and laser power were used to adjust the intensity. At each wavelength the open-circuit and in-circuit (−0.3 V vs. SCE) emission intensity and the photocurrent at −0.3 V vs. SCE were measured. These measurements were made without disturbing the PEC geometry by using a switch on the potentiostat to go from out of circuit to in circuit. Photocurrent was recorded on the Varian recorder, laser intensity on the Scientech-Heath combination, and emission intensity on a Houston Model 2000 x-y recorder (time base mode).

***iLV* Curves.** The PEC was set up in the emission spectrometer in standard three-electrode geometry. A PAR 175 programmer was used in conjunction with the potentiostat to sweep the electrode potential between preset values. The photocurrent vs. voltage curve was displayed on the Houston x-y recorder. Simultaneously, the emission intensity was continuously monitored at λ_{max} on the Varian recorder. Electrode potential was generally swept at ~13 mV/s from −0.3 V vs. SCE negative to the onset of cathodic current at which point the trace was reversed. The incident laser intensity was recorded throughout the trace by splitting part of the beam into the Scientech power meter and displaying its output on the Heath recorder. The laser intensity generally varied by no more than ±5%. These experiments were often repeated at several laser excitation wavelengths and intensities, at different sweep rates, point by point at ~100-mV intervals, and with pulsing between potentials. The small size of the emission compartment precluded accurate measurement of the absolute incident light intensity in the emission spectrometer. Consequently, light intensity was determined by reassembling the PEC outside the emission spectrometer and measuring the intensity which produced the same i-V properties with the Tektronix radiometer.

Open-Circuit Luminescence and Photopotential. A single-crystal 100 ppm CdS:Te electrode was positioned in polysulfide electrolyte in the emission spectrometer. The photoelectrode, high-impedance Varian recorder, and a Pt foil electrode were connected in series. Simultaneously, the open-circuit photopotential and emission intensity (~600 nm) were continuously monitored on the Varian and Houston (time base mode) recorders, respectively, as a function of 501.7- and 514.5-nm laser intensity. The relative intensity was varied by laser power and filter solution path length and measured by splitting part

of the beam into the Tektronix radiometer. Dark potentials and emission intensities of zero were maintained throughout the experiment. Absolute incident light intensities could be estimated for 514.5 nm by reassembling the cell outside the spectrometer as described above in the iLV discussion; for 501.7-nm excitation the solution absorbance permits only an upper limit on intensity.

Efficiency. Extraction of parameters relating to optical to electrical energy conversion efficiency from i–V curves has been described.[4a-c] An estimate of emissive efficiency was made by mounting ~0.25 cm^2 × 1 mm CdS:Te and CdS:Ag samples along their edge. The electrodes were positioned with a Pt wire counterelectrode in a thin 35 × 25 × 2 mm glass cell. The Tektronix radiometer was placed behind the electrode and masked so that scattered light from the laser, incident on the electrode front surface, would not be detected. Energy conversion was estimated by placing the radiometer in front of the cell to record incident intensity, then positioning it behind the cell to record emitted intensity which was scaled up by the fraction of emitted light sampled. The experiment was then repeated after (poly)sulfide electrolyte had been added to the cell. Both the unexpanded and an expanded, masked beam of equivalent power gave similar results.

Low-Temperature Spectra. Emission spectra at 77 K were obtained by placing doped CdS samples of irregular shape in a 15 cm × 7 mm o.d. tube inserted into a Dewar designed to fit into the emission spectrometer chamber. The sample was cooled with liquid N_2, and the emission spectra were recorded with laser excitation. Condensation of water on the Dewar was prevented by continuously purging the sample compartment with N_2. Without disturbing the geometry, the liquid N_2 was allowed to evaporate and the spectra were recorded at 15-min intervals as the sample warmed to 295 K. The incident intensity was constant throughout as determined by splitting the beam into the Scientech power meter and recording the output on the Heath recorder. A crude estimate of the relative photons emitted at the two temperatures (in error owing to the altered emission spectral distribution) was made from the areas under the emission curves.

Electroabsorption. An HCl-polished sample of single-crystal 100 ppm CdS:Te was obtained as a glass-mounted wedge of variable thickness from Cleveland Crystals. At its thinnest point, the sample was colorless to the eye but luminesced brightly upon laser excitation. Electrical contact was established at a thick corner of the wedge in the usual manner, and the sample was placed in polysulfide electrolyte in the standard three-electrode geometry. The unexpanded 514.5-nm laser beam partially penetrated the sample, and this intensity (0.42 mW/cm^2, 2.2% T) was measured by the Tektronix radiometer placed ~4 cm behind it and filtered (Melles Griot 041) to remove the emitted light. Electrode potential was then varied from −0.3 V vs. SCE to the onset of cathodic current in 100-mV increments with the potentiostat. The Tektronix output was continuously displayed on the Varian recorder. Laser output was constant (±5%) as determined by the Scientech-Heath combination.

Acknowledgment. We are grateful to the Office of Naval Research and the Research Corporation for support of this work. Rodney Schreiner, David Morano, and Daniel Bilich are acknowledged for their assistance with some of the measurements.

References and Notes

(1) (a) Nozik, A. J. *Annu. Rev. Phys. Chem.* **1978,** *29,* 189. (b) Wrighton, M. S. *Acc. Chem. Res.* **1979,** *12,* 303.
(2) Ellis, A. B.; Karas, B. R. *J. Am. Chem. Soc.* **1979,** *101,* 236.
(3) (a) Ellis, A. B.; Karas, B. R. *Adv. Chem. Ser.* **1979,** *184,* 185. (b) "Abstracts of Papers", 176th National Meeting of the American Chemical Society, Miami Beach, Fla., Sept. 1978; American Chemical Society; Washington, D.C., 1978; No. 65.
(4) (a) Ellis, A. B.; Kaiser, S. W.; Wrighton, M. S. *J. Am. Chem. Soc.* **1976,** *98,* 1635. (b) *Ibid.* **1976,** *98,* 6855. (c) Ellis, A. B.; Kaiser, S. W.; Bolts, J. M.; Wrighton, M. S. *Ibid.* **1977,** *99,* 2839. (d) Hodes, G.; Manassen, J.; Cahen, D. *Nature (London)* **1976,** *261,* 403. (e) Miller, B.; Heller, A. *Ibid.* **1976,** *262,* 680. (f) Noufi, R. N.; Kohl, P. A.; Bard, A. J. *J. Electrochem. Soc.* **1978,** *125,* 375. (g) Minoura, H.; Tsuiki, M., Oki, T. *Ber. Bunsenges. Phys. Chem.* **1977,** *81,* 588. (h) Heller, A.; Chang, K. C.; Miller, B. *J. Electrochem. Soc.* **1977,** *124,* 697. (i) Minoura, H.; Tsuiki, M. *Electrochim. Acta* **1978,** *23,* 1377. (j) Tsuiki, M.; Minoura, H.; Nakamura, T.; Ueno, Y. *J. Appl. Electrochem.* **1978,** *8,* 523. (k) Ginley, D. S.; Butler, M. A. *J. Electrochem. Soc.* **1978,** *125,* 1968.
(5) (a) Gerischer, H. *J. Electroanal. Chem.* **1975,** *58,* 263. (b) "Physical Chemistry: An Advanced Treatise", Vol. 9A; Eyring, H., Henderson, D., Jost, W., Eds.; Academic Press: New York, 1970; Chapter 5.
(6) (a) Bard, A. J.; Wrighton, M. S. *J. Electrochem. Soc.* **1977,** *124,* 1706. (b) Gerischer, H. *J. Electroanal. Chem.* **1977,** *82,* 133.
(7) Fujishima, A.; Brilmyer, G. H.; Bard, A. J. In "Semiconductor Liquid-Junction Solar Cells", Heller, A., Ed.; Electrochemical Society: Princeton, N.J., 1977; Vol. 77-3, p 172.
(8) (a) Memming, R. *J. Electrochem. Soc.* **1969,** *116,* 786. (b) Beckmann, K. H.; Memming, R. *Ibid.* **1969,** *116,* 368.
(9) Petermann, G.; Tributsch, H.; Bogomolni, R. *J. Chem. Phys.* **1972,** *57,* 1026.
(10) Gerischer, H.; Gobrecht, J. *Ber. Bunsenges. Phys. Chem.* **1978,** *82,* 520.
(11) Noufi, R. N.; Kohl, P. A.; Rogers, J. W. Jr.; White, J. M.; Bard, A. J. *J. Electrochem. Soc.* **1979,** *126,* 949.
(12) Heller, A.; Schwartz, G. P.; Vadimsky, R. G.; Menezes, S.; Miller, B. *J. Electrochem. Soc.* **1978,** *125,* 1156.
(13) Dutton, D. *Phys. Rev.* **1958,** *112,* 785.
(14) Cuthbert, J. D.; Thomas, D. G. *J. Appl. Phys.* **1968,** *39,* 1573.
(15) Roessler, D. M. *J. Appl. Phys.* **1970,** *41,* 4589.
(16) Moulton, P. F. Ph.D. Dissertation, Massachusetts Institute of Technology, 1975.
(17) Cuthbert, J. D. *J. Appl. Phys.* **1971,** *42,* 739.
(18) (a) Aten, A. C.; Haanstra, J. H. *Phys. Lett.* **1964,** *11,* 97. (b) Aten, A. C.; Haanstra, J. H.; deVries, H. *Philips Res. Rep.* **1965,** *20,* 395.
(19) (a) Colbow, K.; Yuen, K. *Can. J. Phys.* **1972,** *50,* 1518. (b) Brown, M. R.; Cox, A. F. J.; Shand, W. A.; Williams, J. M. *J. Lumin.* **1970,** *3,* 96. (c) Woodbury, H. H. *J. Appl. Phys.* **1965,** *36,* 2287. (d) Klick, C. C. *J. Opt. Soc. Am.* **1951,** *41,* 816. (e) Lambe, J.; Klick, C. C. *Phys. Rev.* **1955,** *98,* 909. (f) Vydyanath, H. R.; Kröger, F. A. *J. Phys. Chem. Solids* **1975,** *36,* 509. (g) Kröger, F. A.; Vink, J. H.; van den Boomgard, J. *Z. Phys. Chem. (Leipzig)* **1969,** *203,* 1.
(20) Kolb, D. M.; Gerischer, H. *Electrochim. Acta* **1973,** *18,* 987.
(21) (a) Ellis, A. B.; Bolts, J. M.; Kaiser, S. W.; Wrighton, M. S. *J. Am. Chem. Soc.* **1977,** *99,* 2848. (b) Ellis, A. B.; Bolts, J. M.; Wrighton, M. S. *J. Electrochem. Soc.* **1977,** *124,* 1603. (c) Legg, K. D.; Ellis, A. B.; Bolts, J. M.; Wrighton, M. S. *Proc. Natl. Acad. Sci. U.S.A.* **1977,** *74,* 4116. (d) Bolts, J. M.; Wrighton, M. S. *J. Am. Chem. Soc.* **1978,** *100,* 5257. (e) Bolts, J. M.; Bocarsly, A. B.; Palazzotto, M. C.; Walton, E. G.; Lewis, N. S.; Wrighton, M. S. *Ibid.* **1979,** *101,* 1378.
(22) Tanenbaum, M. "Semiconductors", *ACS Monogr.* **1959,** *No. 140,* p 87.
(23) Calvert, J. G.; Pitts, J. N. Jr. "Photochemistry"; Wiley: New York, 1966; p 798 ff.
(24) Hutson, A. R. "Semiconductors", *ACS Monogr.* **1959,** *No. 140,* p 579.
(25) Blossey, D. F.; Handler, P. In "Semiconductors and Semimetals", Willardson, R. K., Beer, A. C., Eds.; Academic Press: New York, 1972; Vol. 9, Chapter 3.
(26) (a) Mead, C. A.; Spitzer, W. G. *Phys. Rev. Lett.* **1963,** *10,* 471. (b) Spitzer, W. G.; Gershenzon, M.; Frosch, C. T.; Gibbs, D. F. *J. Phys. Chem. Solids* **1959,** *11,* 339.
(27) Leverenz, H. W. "An Introduction to Luminescence of Solids"; Wiley: New York, 1950.
(28) These assignments are based on Auger and ESCA studies of single-crystal 100 ppm CdS:Te: Bilich, D. K.; Morano, D. J.; Karas, B. R.; Ellis, A. B., unpublished results.